Intercellular communication between glioma and innate immune cells

Abels, E.R.

Chapter 2

Directly visualized glioblastoma-derived extracellular vesicles transfer RNA to microglia/macrophages in the brain

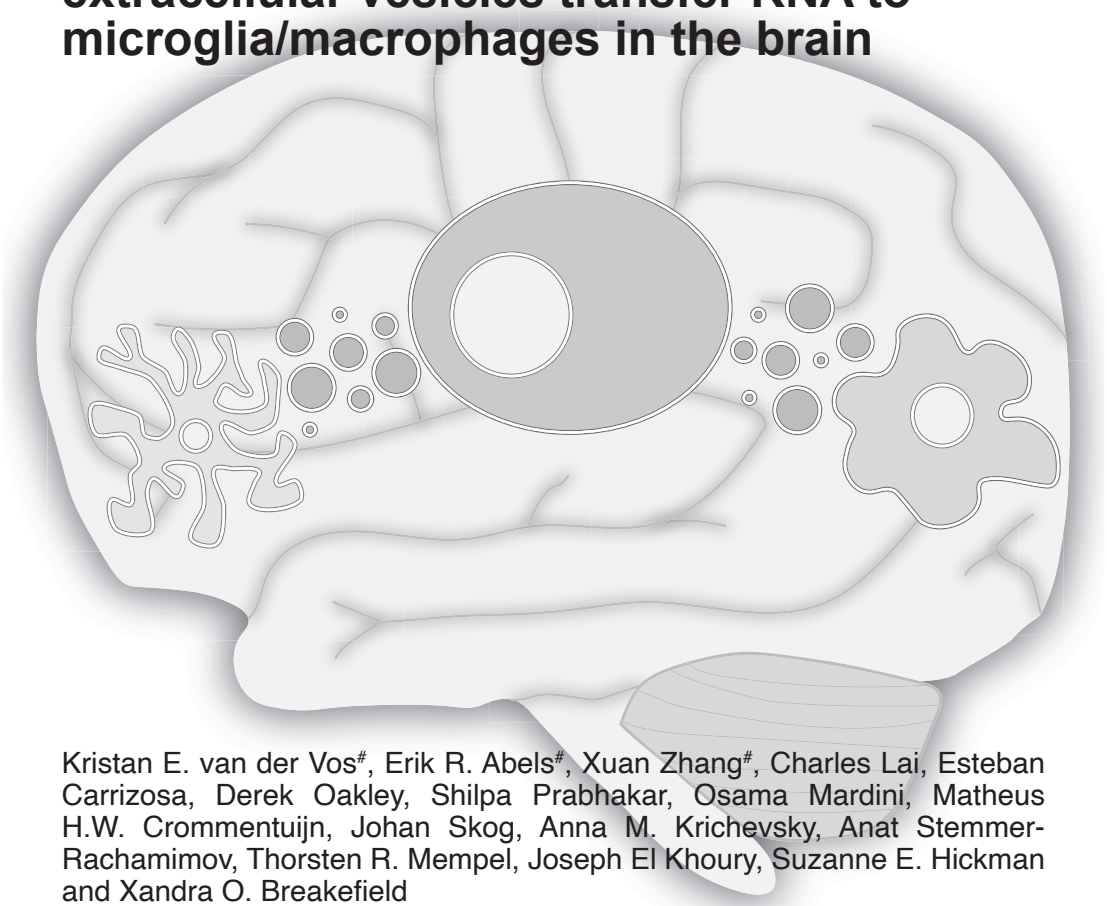

Kristan E. van der Vos[#], Erik R. Abels[#], Xuan Zhang[#], Charles Lai, Esteban Carrizosa, Derek Oakley, Shilpa Prabhakar, Osama Mardini, Matheus H.W. Crommentuijn, Johan Skog, Anna M. Krichevsky, Anat Stemmer-Rachamimov, Thorsten R. Mempel, Joseph El Khoury, Suzanne E. Hickman and Xandra O. Breakefield

[#] These authors contributed equally to this work.

Neuro Oncology. 2016

Abstract

To understand the ability of gliomas to manipulate their microenvironment, we visualized the transfer of vesicles and the effects of tumor-released extracellular RNA on the phenotype of microglia in culture and *in vivo*. Extracellular vesicles (EVs) released from primary human glioblastoma (GBM) cells were isolated and microRNAs (miRNAs) were analyzed. Primary mouse microglia were exposed to GBM-EVs and their uptake and effect on proliferation and levels of specific miRNAs, mRNAs, and proteins was analyzed. For *in vivo* analysis mouse glioma cells were implanted in the brains of mice and EV release and uptake by microglia and monocytes/macrophages was monitored by intravital two-photon microscopy, immunohistochemistry and FACS analysis, as well as RNA and protein levels. Microglia avidly took up GBM-EVs vesicles, leading to increased proliferation, and shifting of their cytokine profile towards immune suppression. High levels of miR-451/miR-21 in GBM-EVs were transferred to microglia with a decrease in the miR-451/miR-21 target *c-Myc* mRNA. In *in vivo* analysis, we directly visualized release of EVs from glioma cells and their uptake by microglia and monocytes/macrophages in brain. Dissociated microglia and monocytes/macrophages from tumor-bearing brains revealed increased levels of mi-R21 and reduced levels of *c-Myc* mRNA. Intravital microscopy confirms the release of EVs from gliomas and their uptake into microglia and monocytes/macrophages within the brain. Our studies also support functional effects of GBM-released EVs following uptake into microglia associated in part with increased miRNA levels, decreased target mRNAs and encoded proteins, presumably as a means for the tumor to manipulate its environs.

Introduction

Glioblastoma (GBM) account for 12-15% of intracranial tumors, with an incidence of 2-3 new cases per 100,000 people per year(Johnson and O'Neill, 2012). The standard-of-care, consisting of surgical resection combined with chemotherapy and radiotherapy, provides a median survival of about 14 months from diagnosis(Johnson and O'Neill, 2012). Extensive evidence indicates that cancer cells can subvert surrounding normal cells to promote tumor growth, angiogenesis, invasion and metastases(Coniglio and Segall, 2013; D'Asti et al., 2012). GBM tumors rarely metastasize, but they exert influence over endogenous cell types within the brain, including microglia, macrophages, astrocytes, oligodendrocytes, neurons, and endothelial cells(D'Asti et al., 2012). In addition, blood monocytes enter the tumor-bearing brain and differentiate into macrophages in association with GBMs(Kushchayev et al., 2014). GBM tumor cells attract microglia and monocytes/

macrophages by secreting chemokines, cytokines and matrix proteins, and stimulate their proliferation resulting in their abundance within the tumor mass. Following interaction with tumor cells, microglia/macrophages show phenotypic activation changes that direct them towards an immunosuppressive state with increased release of cytokines, such as IL-10 and TGF-β, and up-regulation of arginase-1 (*Arg-1)* and matrix metalloprotease which support growth and invasion associated with tumor progression(Coniglio and Segall, 2013; Li and Graeber, 2012; Wurdinger et al., 2014).

GBM tumors are known to mold their environment to their advantage by secretion of proteins and the display of cell surface ligands, and with increasing evidence supporting transfer of instructional extracellular RNA (exRNA) and proteins/lipids contained within extracellular vesicles (EVs – including exosomes, microvesicles, ectosomes), ribonucleoproteins (RNPs) and high-density lipoproteins (HDLs) (Arroyo et al., 2011; Skog et al., 2008; Vickers et al., 2011). The important role of EVs in cancer progression has been well documented(D'Asti et al., 2012; Peinado et al., 2012). Once released, EVs can be internalized into "recipient cells", potentially delivering genetic information to multiple cell types in the tumor microenvironment. This constitutes a new type of intercellular communication – the transfer of informative RNA between cells. Recent, studies support the functional transfer of microRNA (miRNA) and other non-coding RNAs from tumor cells to normal cells(Bronisz et al., 2014; Li et al., 2013a; Zhou et al., 2014).

We investigated the activity of exRNA released from glioma cells and taken up by microglia and macrophages as a means by which tumor cells manipulate normal cells in their microenvironment. We monitored phenotypic changes in microglia exposed to isolated human GBM EVs in culture, as well as the uptake of EVs and specific miRNAs and their effects on target mRNAs in an intracranial mouse glioma model. We focused on two miRNAs, miR-451 and miR-21, which naturally have very high levels in the EVs produced by primary GBM cells. Exposure of microglia in culture to these GBM-EVs elevated levels of these miRNAs and decreased levels of a common mRNA target encoding c-Myc. Further, utilizing a syngeneic mouse glioma model expressing red fluorescent protein (RFP) in tumor cells and their EVs, and green fluorescent protein (GFP) in microglia and monocytes/macrophages, we found that infiltration of tumors by these cells was associated with their uptake of labeled tumor EVs, as visualized with multi-photon *in vivo* microscopy. FACS sorting of brain cells revealed increased levels of miR-21, decreased levels of *c-Myc* mRNA and increases in the activation-related *Arg-1* mRNA. Our results are consistent with functional transfer of miRNAs from glioma cells to surrounding microglia and macrophages via EVs, as a means of modulating their phenotype, albeit EVs contain many types of RNAs and proteins which, along with the secretome of glioma cells, probably exerts a combinatorial effect.

Results

GBM-derived EVs are internalized by microglia

Two primary human GBM cell lines, GBM 11/5 (GBM1) and GBM 20/3 (GBM2) have been previously characterized for mRNA content in cells(Skog et al., 2008), with the most highly expressed mRNAs being consistent with the mesenchymal subtype(Verhaak et al., 2010). Both lines released large quantities of EVs (mg protein, **Supplementary Fig. S1A**, and number of particles, **Supplementary Fig. S1C**), the majority of which were 100-200 nm in diameter (**Supplementary Fig. S1D**) and contained the EV marker acetylcholinesterase (**Supplementary Fig. S1B**). Variations in the number of EVs released by different GBM/glioma lines has been documented(de Vrij et al., 2015). GBM2 cells which released more EVs than GBM1 cell were used in most experiments. Vesicle internalization by microglia was assessed by exposing primary neonatal mouse microglia to isolated EVs from GBM2 cells expressing membrane-tagged GFP (palmGFP). After 24h most microglia had taken up many fluorescently-tagged EVs (**Fig. 1A**).

Figure 1. Exposure of primary mouse microglia to GBM-EVs directs them towards a tumor-associated phenotype. **(A)** EVs isolated from GBM2 cells expressing palmGFP were incubated for 24h with primary mouse microglia, followed by confocal fluorescent microscopy using a 20X objective and DAPI staining. **(B)** Microglia were exposed for 48h to GBM-EVs (black bars) and compared to untreated cells (white bars). Cytokines increasing over 50% are indicated by black arrowheads, those decreasing by over 50% by white arrowheads. **(C)** Microglia were exposed to GBM-EVs every 24h for 5 days. Viability was measured after 7 days and compared to untreated cells. (mean ± SEM * $p < 0.05$). **(D)** *Arg-1* mRNA was quantitated in microglia after exposure to GBM-EVs for 24 and 48h (fold change presented (n=2)) (Scale bar, 20 μm in A)

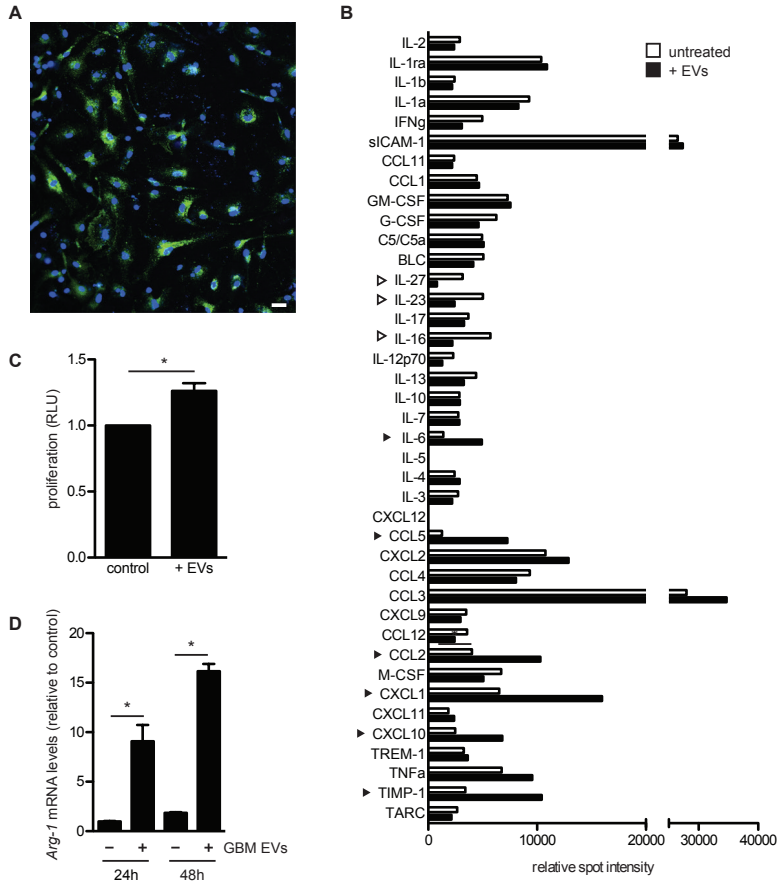

Uptake of GBM-derived EVs changes the phenotype of microglia

First, we tested whether uptake of EVs could change the cytokines produced by mouse microglia. To mimic the constant exposure of microglia to EVs in the tumor microenvironment, microglia were incubated with freshly isolated GBM-EVs every 24h over 5 days. The relative levels of 40 different cytokines and chemokines was compared in microglia exposed to EVs compared to unexposed cells using a Cytokine Antibody Array (R&D Systems). Densitometric analysis showed six cytokines that were more than 50% up-regulated following GBM-EV exposure, comprising TIMP-1, chemokines CXCL10, CXCL1, CCL2 and CCL5, and cytokine IL-6 (**Fig. 1B**). Of these up-regulated cytokines - TIMP-1 is involved in extracellular matrix degradation(Ries, 2014); and the chemokines CXCL10, CXCL1, CCL2 and CCL5 and the cytokine IL-6 all induce glioma growth(Coniglio and Segall, 2013). In contrast, three cytokines involved in induction of immune

responses were more than 50% down-regulated - IL-16 (orchestrates immune response)(Richmond et al., 2014), IL-23 (promotes inflammation) and IL-27 (together with IL-23 enhances immunologic functions)(Cocco et al., 2012). Thus, exposure/uptake of GBM-EVs changes the cytokine secretion profile of microglia towards a phenotype that promotes growth and invasion of GBM cells, while decreasing the immune response. In addition, we found that GBM-EVs contain high levels of TGF-β (**Supplementary Fig. S2A**). Exposure of mouse microglia to GBM-EVs did not increase mouse Tgf-β1 mRNA (**Supplementary Fig. S2B**) but did increase intracellular levels of TGF-β presumably through uptake of GBM-EVs (**Supplementary Fig. S2C**).

Second, we found that the presence of GBM-EVs increased the proliferation of mouse microglia by about 40% over 7 days (**Fig. 1C**). Further, exposure of microglia to GBM-EVs increased levels of *Arg-1* (almost 10-fold) after 24 and 48h (**Fig. 1D**), consistent with an activated tumor-associated phenotype.

Specific miRNA content in GBM cells and EVs compared to microglia.

Micro-array analysis on 1146 different miRNAs was performed on primary human GBM cell lines, GBM1 and GBM2, and on EVs isolated from conditioned medium from these cells (**Fig. 2A**). Many miRNAs were expressed at similar levels in cells and EVs, while some showed a distinct difference in levels (**Fig. 2B**). Two of the most abundant miRNAs in vesicles were miR-451, which was over 40-fold higher in EVs than cells (**Fig. 2C**), and miR-21, a known oncomir(Krichevsky and Gabriely, 2009), which had similarly high levels in both cells and EVs (**Fig. 2B**). We verified the expression levels of miR-21 and miR-451 in primary GBM1 and GBM2 cells and GBM-EVs by TaqMan® assays. Relative levels of miR-21 were not significantly different between cells and EVs (**Fig. 3A, Supplementary Fig. S3A**), whereas miR-451 levels were 1,000 to 10,000-fold higher in the vesicle fraction compared to cells (**Fig. 3B, Supplementary Fig. S3B**).

Figure 2. **EVs secreted by GBM cells are enriched for many miRNAs. (A)** miRNA array analyses on two human primary GBM cell lines and EVs secreted by them was performed and a heat map was created using CIMminer (Weinstein et al., 1997). **(B)** Ratio of intensity in EVs compared to cells is presented in log2 scale for all 1146 miRNAs. **(C)** Comparison of the 20 most highly enriched miRNAs in EVs from GBM1 and GBM2 cells.

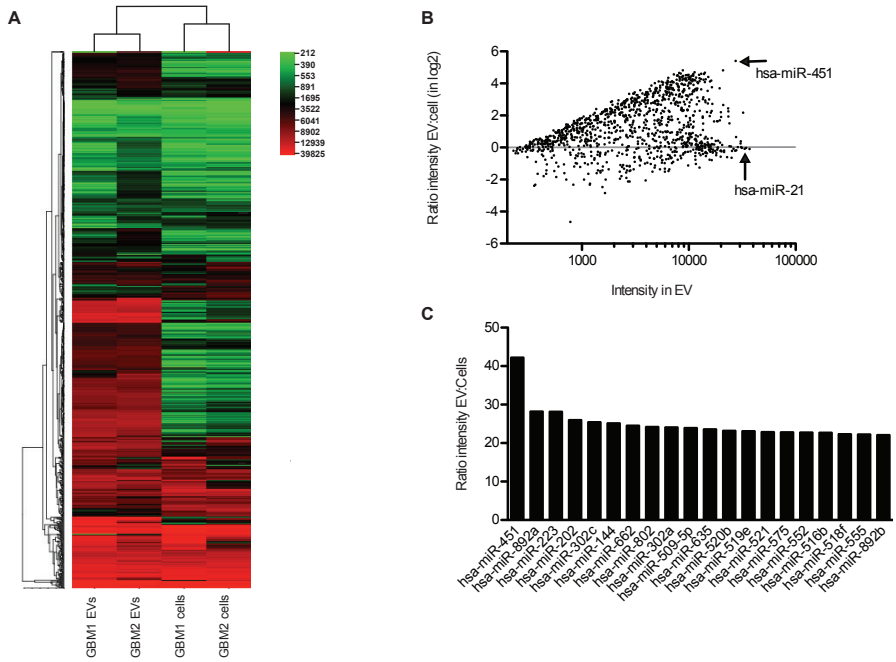

Microglia were chosen as the recipient normal brain cell based on their importance to tumor growth(Coniglio and Segall, 2013; Li and Graeber, 2012; Wurdinger et al., 2014), relative ease of culture of primary cells from mouse and human sources, and the availability of transgenic mice with GFP+ microglia/macrophages(Jung et al., 2000). GBM cells are known to release abundant levels of small non-coding RNAs, such as miRNAs(Manterola et al., 2014). Given the ability of EVs to carry intact miRNAs we evaluated whether this extracellular miRNA could serve as a mechanism by which GBM cells could manipulate microglia. We hypothesized that the intercellular transfer of miRNAs from GBM cells to microglia might contribute to their phenotypic changes.

Sucrose density gradient centrifugation was used to resolve components of the GBM-EV preparation on the basis of buoyant density (**Fig. 3C**). Density fractions were analyzed for the presence of the exosomal marker, ALIX(Bobrie et al., 2012), as well as for miRNA levels. ALIX was most prominent in the fractions with a density of 1.20, 1.25 and 1.30 mg/ml (**Fig. 3C**), typical of classical exosomes. miR-21 and miR-451 co-localized with the exosome-marker ALIX but were also found in denser fractions which were negative for ALIX. These denser fractions might contain other types of EVs, RNPs or HDL particles.

We also evaluated the endogenous levels of miR-451 and miR-21 in mouse primary microglia. miR-21 and miR-451 had higher Ct levels in mouse microglia

compared to GBM-EVs (**Fig. 3, D & E**). For miR-21 the Ct difference between GBM-EVs and mouse microglia was 4.8 (equivalent to 32-fold), and for miR-451 this differential Ct was 11.2 (equivalent to about 2000-fold). Note the much higher levels of miR-21, as compared to miR-451, in both GBM cells and EVs. The high levels of these miRNAs in GBM-EVs compared to the low levels in microglia was exploited to monitor functional transfer of these miRNAs from GBM cells into microglia via exRNA.

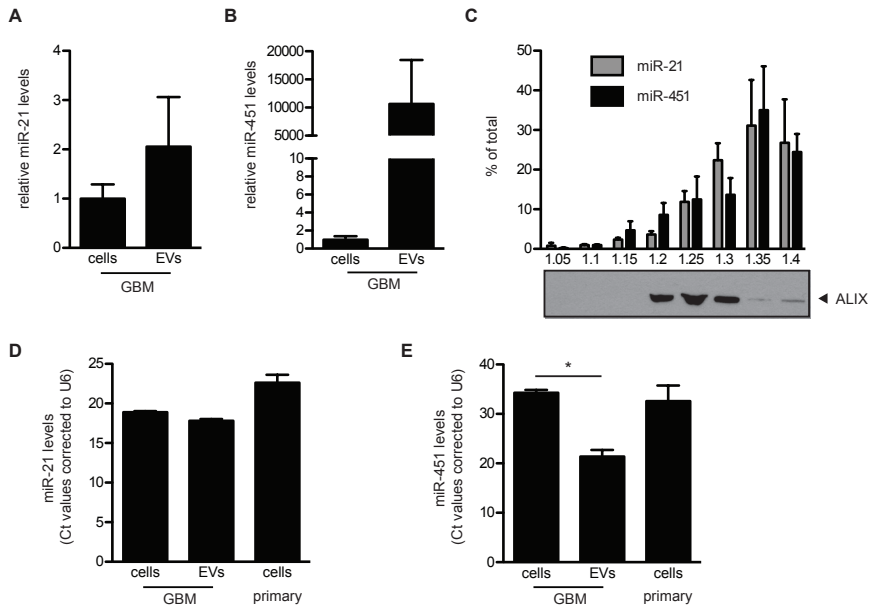

Figure 3. GBM cells release EVs enriched for miR-451 and miR-21 compared to microglia. (A, B) Levels of miR-21 **(A)** and miR-451 **(B)** in EVs and GBM2 cells were analyzed (mean ± SEM (n=2)). **(C)** Isolated GBM-EVs were separated on a sucrose density gradient. Levels of miR-21 and miR-451 in the different fractions were analyzed (mean ± SEM (n=2)). Protein levels of ALIX were analyzed by western blotting. **(D, E):** Levels of miR-451(**D**) and miR-21 (**E**) in GBM cells, GBM-EVs and primary mouse microglia were analyzed (Ct values presented (n=2).

GBM-EV mediated transfer of miR-451/miR-21 to microglia and decrease in c-Myc mRNA

To investigate whether GBM-EVs were capable of transferring miRNAs between cells, miR-451 and miR-21 levels in mouse microglia were monitored 24 and 48h after exposure to GBM-EVs. Initially, analysis was carried out using the murine microglial cell line KW3 with a trend seen towards higher levels of miR-21 and miR-451 after uptake of GBM-EVs (**Supplementary Fig. S3C & D**). To more closely mimic the *in vivo* situation, we tested primary mouse microglia, in which case levels

of miR-21 significantly increased 1.3- and 5-fold after 24 and 48h of exposure to GBM-EVs, respectively (**Fig. 4A**). Strikingly, levels of miR-451 in primary microglia increased up to 50-fold compared after 48h exposure (**Fig. 4B**).

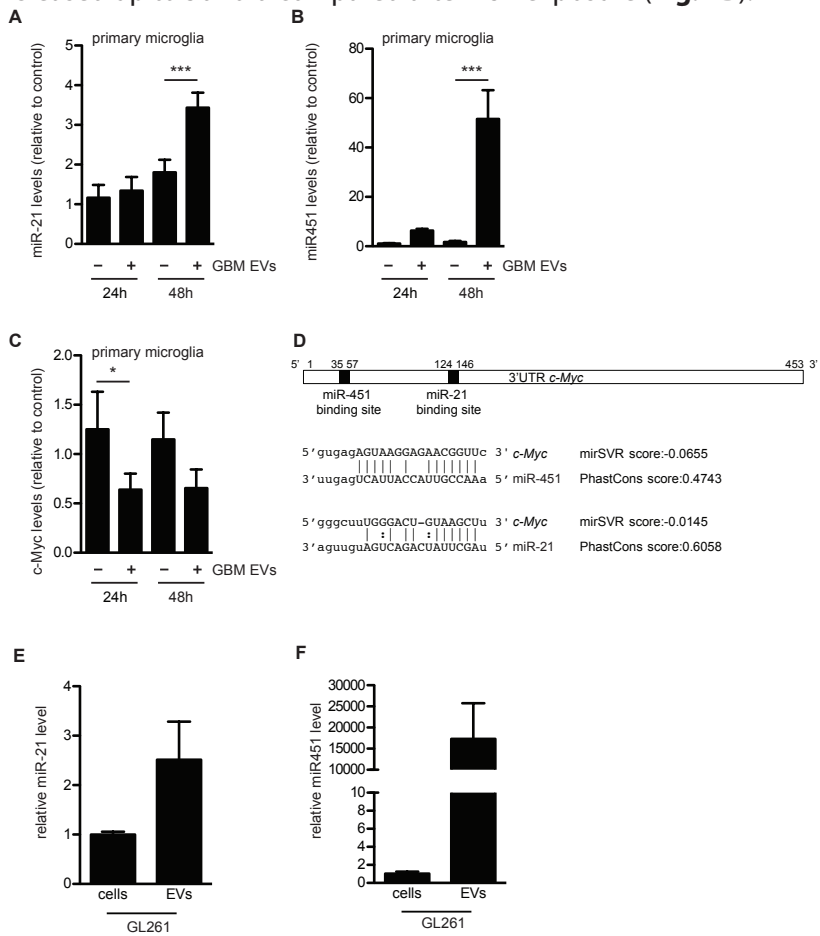

Figure 4. GBM-derived EVs increase miR-21 and miR-451 levels and decrease *c-Myc* mRNA levels in primary mouse microglia. (**A, B**): Primary microglia were exposed to GBM-EVs for 24 and 48h. Levels of miR-21 (**A**) and miR-451 (B) were quantitated (mean ± SEM (n=5), *** $p < 0.001$). (**C**) mRNA levels of *c-Myc* were measured (mean ± SEM (n=6), * $p < 0.05$). (**D**) Schematic representation of 3'UTR of mouse *c-Myc* mRNA with miR-451 and miR-21 binding sites predicted using computational microRNA target software (http://www.microrna.org). (**E, F**): Levels of miR-21 (**E**) and miR-451 (**F**) in GL261 cells and EVs released from them were analyzed (fold change presented (n=2)).

In addition, human adult primary microglia exposed to labeled GBM-EVs rapidly took up the vesicles (**Supplementary Fig. 6A**) and also displayed notably increased levels of miR-21 (1.5-fold) and miR-451 (4-fold) (**Supplementary Fig. S6B & C**). The GBM-EV-mediated increase in miR-451 and miR-21 levels in mouse

microglia was partially blocked by heparin, which interferes with EV uptake (**Supplementary Fig. S4**)(Atai et al., 2013). These findings support our contention that the increase in miRNA levels seen in microglia after GBM-EV exposure are due, at least in part, to uptake of EVs containing these miRNA.

Next, we examined the ability of the transferred miRNAs to down-regulate target mRNAs. A number of targets are regulated by miR-451, including *Cab39, Mif,* and *c-Myc* (Meng et al., 2007; Pan et al., 2013). The levels of the miR-451 target-mRNAs - *Cab39* and *Mif* and of the miR-21 target-mRNA - *Pten* did not change significantly in primary mouse microglia upon exposure to GBM-EVs. Using target prediction software we found that the 3'UTR of the *c-Myc* mRNA contains binding sites for both miR-451 and miR-21 (http://www.microrna.org) (Betel et al., 2010),and levels of this common target-mRNA - *c-Myc* were significantly down-regulated by about 50% when microglia were incubated with GBM-EVs (**Fig. 4D&C**). This increased sensitivity of *c-Myc* mRNA in microglia to miRNA inhibition may reflect both the low levels of this mRNA in these cells, as compared to the other target mRNAs tested (**Supplementary Fig. S5E**), as well as its being a target for both miR-451 and miR-21 (**Fig. 4D**; **Supplementary Fig. S5D**). When we performed the same experiment using human microglia exposed to GBM-EVs, marked decreases in mRNA levels of *c-MYC, MIF, and CAB39* were noted (**Supplementary Fig. S6D-G**). For mouse microglia we also evaluated the relative levels of proteins encoded in these target mRNAs by western blot analysis, with apparent decreases after GBM-EV exposure for c-Myc, Pten and Mif, but not Cab39 (**Supplementary Fig. S5F-I**). Amounts of human microglia were insufficient for western blot analysis.

In vivo assessment of uptake of glioma-derived EVs by brain microglia and monocytes/macrophages.

To investigate whether myeloid cells of the tumor brain stroma take up glioma-derived EVs *in vivo*, we used the syngeneic GL261 model(Ausman et al., 1970). EVs derived from GL261 cells have elevated levels of miR-21 and miR-451, as compared to these tumor cells (**Fig. 4E & F**) and these GL261-EVs are taken up by mouse microglia in culture (**Supplementary Fig. S2D**). GL261-Fluc-mC-palmtdT tumors releasing red fluorescent EVs were established in the brains of *C57BL/6* wt and *C57BL/6 CX3CR1*$^{GFP/+}$ mice, with the latter expressing GFP in microglia and monocyte-derived macrophages(Jung et al., 2000). Multiphoton intravital microscopy analysis of tumors was conducted using cortical brain windows, starting 1 week after tumor implantation. GL261-Fluc-mC-palmtdT tumors produced red fluorescent punctae resembling vesicles or clusters of vesicles that were located directly adjacent to, as well as in the spaces between tumor cells and the stroma (**Fig. 5A, B**). Such vesicles were not present in tumors expressing

soluble fluorescent proteins(Lai et al., 2015) and were therefore likely derived from tdTomato-labeled tumor cell membranes. The apparent sizes of vesicles and vesicle clusters ranged from several micrometers down to below 1 µm. However, detection by fluorescence may, on the one hand, overestimate their actual physical size, and on the other hand, very small vesicles may escape detection by our imaging system. Therefore, visualized vesicles may represent only a fraction of EVs that are produced. As we have observed in other tumor models(Lai et al., 2015), vesicles in central areas of the tumors were mostly stationary (**Supplementary Video S1**), while vesicles in more peripheral areas that were densely populated by *CX3CR1-GFP*$^{+}$ microglia and monocytes/macrophages, displayed more dynamic properties (**Fig. 5B**). Importantly, our recordings revealed that most of the detectable vesicles were located either on the surface or inside of GFP^{+} microglia/monocyte-derived macrophages (**Fig. 5C**) that frequently made intimate contacts with individual tumor cells (**Fig. 5B**, **subpanel 2**), but were in some cases located at some distance from labeled tumor cells. In different fields of view, the frequency of *CX3CR1-GFP*$^{+}$ cells that contained red punctae ranged from 18 and 74%, depending on the tumor area. In most *CX3CR1-GFP*$^{+}$ cells one or two, but in some cases up to 10 individual fluorescent punctae (single vesicles or clusters) could be identified (**Fig. 5D**). Rotation and stacking of GFP^{+} cells confirmed that many red vesicles were within cells.

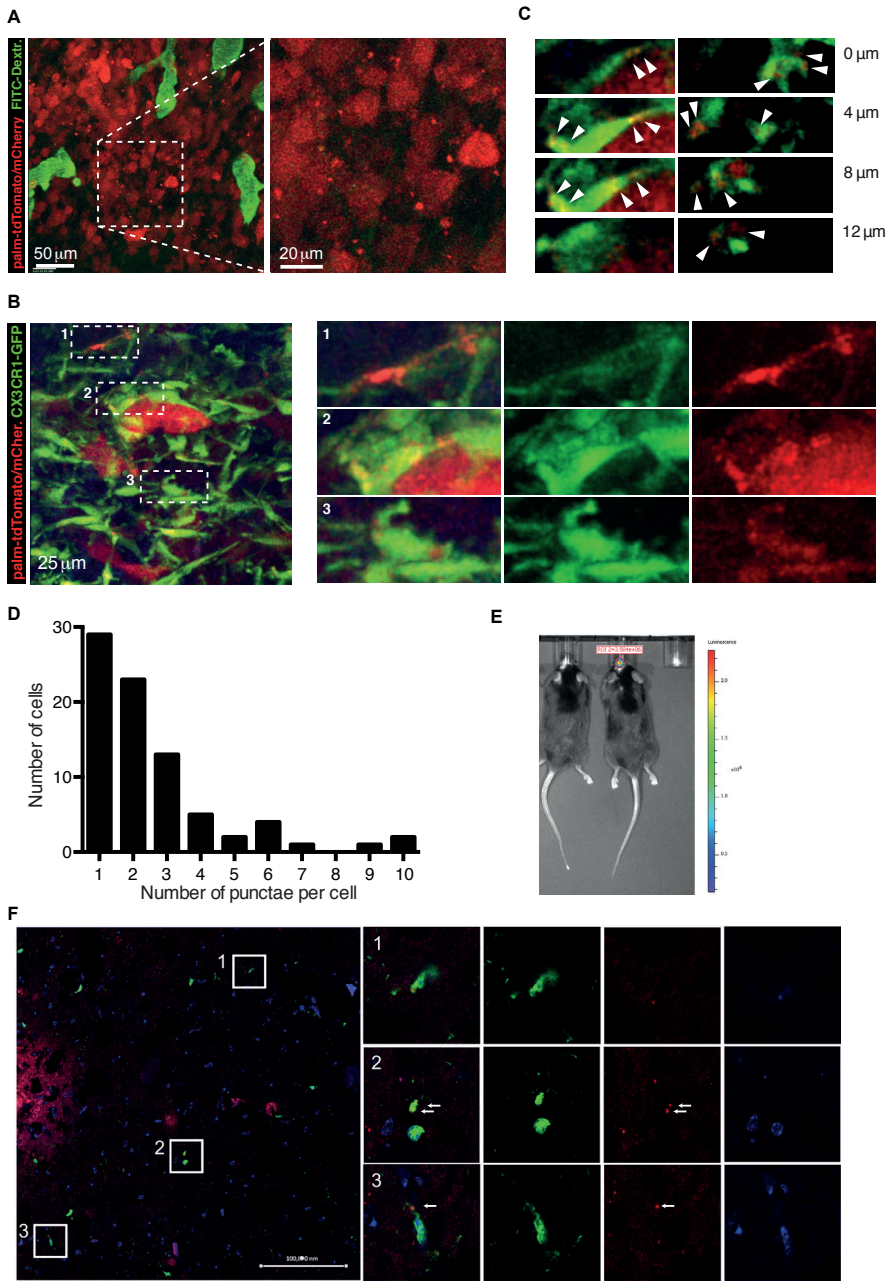

Figure 5. ***In vivo*** **visualization of glioma derived EVs and uptake by microglia/ macrophages**. **(A)** MP-IVM images from a GL261-Fluc-mC-palmtdT in a *C57BL/6* mouse implanted with a brain window. 150 kDa FITC-Dextran was injected i.v. to label the blood vasculature. **(B)** MP-IVM images from a GL261-Fluc-mC-palmtdT tumor in a *CX3CR1*$^{GFP/+}$ mouse brain. Panels on right show magnified subregions of panel on left (**C**) Individual sections highlighting intracellular localization of red punctae. (**D**) Frequency distribution

of number of discernable red punctae per cell. **(E)** Tumor size of GL261-Fluc-mC-palmtdT cells implanted intracranially into *CX3CR1*$^{+/GFP}$ mice monitored by bioluminescence *in vivo* Fluc imaging. Cryosections were performed to visualize *in vivo* EV uptake. Released EV-like entities (palmtdT+) were readily observed around the tumor, as well as within GFP+ cells. Nuclei were visualized by DAPI. Arrows indicated red punctae within GFP+ cells. Bar = 100,000 nm.

In parallel experiments following direct injection of these tumor cells into the cortex of *CX3CR1*$^{GFP/+}$ mouse brains, tumor growth was monitored by *in vivo* bioluminescence imaging (**Fig. 5E**). Mice were sacrificed after 18 days when tumors had formed and either analyzed by immunohistochemistry or used to isolate cells for FACS analyses. Immunohistochemistry of brains of tumor-bearing mice showed influx of GFP+ microglia/macrophages into the periphery of GL261-Fluc-mC-palmtdT tumors (**Fig. 5F**), as well as uptake of "red" tdT-positive vesicles by GFP+ cells.

In parallel, brains of tumor-bearing and control animals were dissociated into single cells, which were resolved by FACS into fractions of tumor cells (red), microglia (high levels of GFP), and monocytes/macrophages (intermediate levels of GFP) (**Fig. 6A**). The numbers of monocytes/macrophages increased in the glioma-bearing brains of mice as compared to control mice. While there was no significant change in the total number of microglia in the brain (**Fig. 6B**), there appeared to be a higher density of these cells associated with tumors (**Fig. 5B**). Interestingly, microglia (and to some extent macrophages) showed a significant increase in red fluorescence (PE-A), consistent with their uptake of mC/palm-TdTomato+ EVs released by the GBM cells *in vivo* (**Fig. 6C**). Analysis of mRNA levels in isolated cell fractions from brains showed enrichment of the mRNA for the microglia marker, *P2ry12*(Hickman et al., 2013) in the microglia population and enrichment of the macrophage marker, *Ccr2* in the monocyte/macrophage population (**Fig. 6D**), confirming the validity of isolation based on GFP intensity. The levels of miR-451 and miR-21 were also measured in the isolated microglia and monocytes/macrophages. While the levels of miR-451 were below detection limits, the levels of miR-21 were 20-fold increased in microglia and 8-fold increased in monocytes/macrophages in tumor-bearing mice as compared to control brains (**Fig. 6E**). Increased levels of miR-21 in microglia and monocytes/macrophages from brains of tumor-bearing mice correlated with a marked decrease in levels of the target *c-Myc* mRNA as compared to controls (**Fig. 6F**), supporting EV-mediated functional transfer of miRNA from glioma to microglia and monocytes/macrophages *in vivo*.

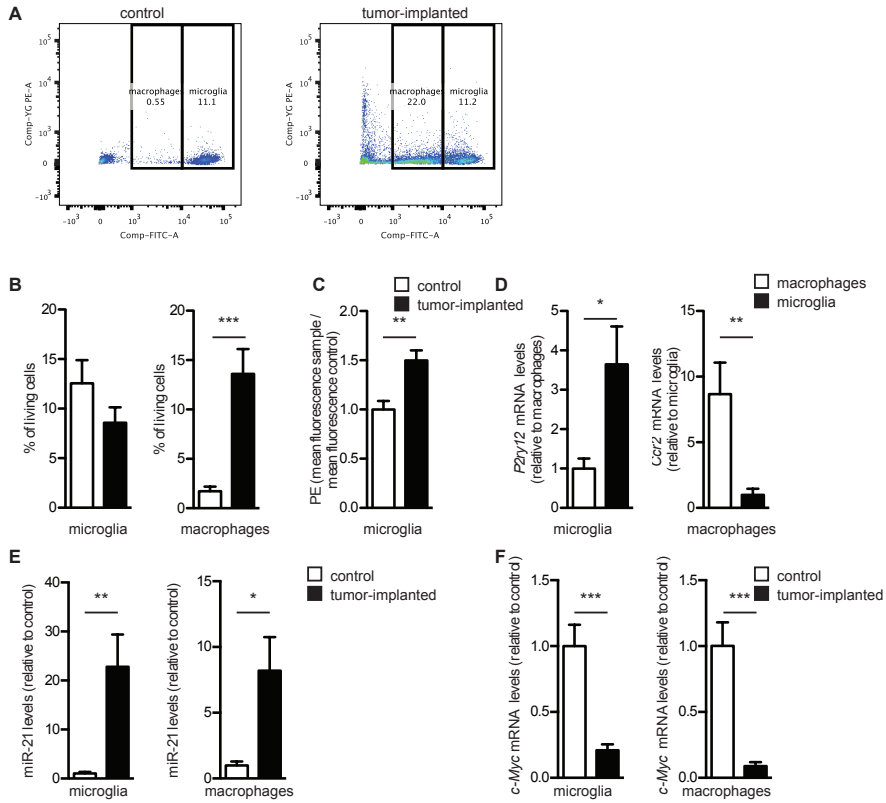

Figure 6. Microglia isolated from brains of mice with glioma show increased levels of miR-21 and decreased *c-Myc* mRNA. (A) Representative images of FACS sorted cells from brains of mice without and with gliomas; macrophages and microglia (GFP+; FITC) and tumor cells (mC/palmtdTomato+; PE-A). **(B)** The % living FAC sorted GFP+ cells from control brains and tumor-implanted brains were determined (mean ± SEM *** $p < 0.001$). **(C)** The PE-A mean fluorescence of sorted microglia from tumor as compared to control brains. (** $p < 0.01$). **(D)** Cells sorted based on GFP+ intensity were analyzed for mRNA levels of *P2ry12* and *Ccr2*. (* $p < 0.05$, ** $p < 0.01$), **(E)** miR-21 levels (* $p < 0.05$, ** $p < 0.01$), and **(F)** *c-Myc* levels (*** $p < 0.001$). **(B-F):** All graphs include a total of 8 control mice and 9 mice implanted with GBM cells (mean± SEM; n=3).

Discussion

Tumors are known to change the phenotype of normal cells in their environs to promote tumor progression, and microglia and macrophages are key players in this process(Li and Graeber, 2012; Wurdinger et al., 2014). Many interactions between gliomas and microglia/macrophages are mediated via chemokines and cytokines in the secretome. The current study supports an additional form of communication in which multipotent miRNAs are transferred from tumor cells

into microglia and macrophages via EVs. Release of fluorescently labeled EVs by glioma cells and uptake by microglia/macrophages within the brain tumor environs were documented *in vivo* in real time using intravital microscopy. Extracellular transfer of miR-451 and miR-21 in glioma-EVs resulted in elevated levels in microglia/macrophages and associated down-regulation of their target mRNAs and encoded proteins, albeit given other RNAs and proteins in these EVs, the effect may be combinatorial.

Here we demonstrate for the first time to our knowledge, using dynamic intravital microscopy, as well as histological analyses, that EVs released from tumor cells are not only taken up by microglia in culture, but also by tumor-associated microglia and monocytes/macrophages in the glioma-bearing brain. Stacking and rotational analysis of intravital images confirmed uptake of vesicles into microglia/macrophages. Consistent with this, dissociation and FACS sorting of these cells from tumor-bearing brains demonstrated that many microglia and monocytes/macrophages have marked levels of red fluorescence, presumably reflecting the uptake of tumor EVs. FACS-isolated microglia and monocytes/macrophages from tumor-bearing animals also showed both an increase in miR-21 levels and a decrease in *c-Myc* mRNA. These *in vivo* findings are consistent with functional transfer of miRNAs from glioma cells to microglia and monocytes/macrophages via exRNA vehicles.

The role of exRNAs in communication between GBM and microglia/ monocytes/macrophages was evaluated both in culture and *in vivo,* with these myeloid-derived cells known to infiltrate brain tumors(Kushchayev et al., 2014) and their density being proportional to glioma grade(Li and Graeber, 2012). Primary GBM cells shed EVs in large numbers(Balaj et al., 2011), and resident brain microglia are very active in endocytosis(Kushchayev et al., 2014). EVs derived from GBM cells were avidly taken up by microglia and monocytes/macrophages in culture and *in vivo* as analyzed by confocal and intravital microscopy, visualizing the internalization of EVs into recipient cells using fluorescent membrane labels(Lai et al., 2015). GBM-EV uptake correlated with changes in microglia phenotype, including increased proliferation, differences in secretion of various cytokines, and increased levels of *Arg-1* mRNA associated with activation. The GBM-EV fraction contained a unique repertoire of miRNAs as compared to GBM cells, with two miRNAs, miR-451 and miR-21 being inherently highly abundant in the EVs. We exploited the low levels of these miRNAs in microglia to demonstrate increases in cellular miR-451 and miR-21 levels conferred by exposure to GBM-EVs, consistent with, but not direct proof of, the transferred miRNAs being responsible for this increase. Exposure of mouse microglia/macrophages to GBM/glioma-EVs also decreased levels of *c-Myc* mRNA both in culture and *in vivo*, presumably through binding of elevated miR-451 and miR-21 to target sites in the 3'UTR of this mRNA. The down-regulation of

c-Myc mRNA in mouse microglia exposed to human GBM-EVs was unexpected as another study reported elevated levels of this message following exposure of rat microglia to conditioned medium from rat glioma cultures(Ellert-Miklaszewska et al., 2013). However, our findings of decreased *c-Myc* mRNA levels in microglia and monocytes/macrophages in glioma-bearing mouse brain are similar to those of another group using the same mouse tumor model(Wei et al., 2013). This suggests that secreted proteins, such as cytokines, and particulate exRNA vehicles, two components of the secretome, have a combinatory effect and may even convey different signals to microglia, which can have either tumor supportive or anti-tumor properties(Gabrusiewicz et al., 2011).

We found a unique repertoire of miRNAs in GBM-EVs compared to GBM cells, supporting a selective loading of RNAs into EVs(Li et al., 2013a). miR-451 was the most highly enriched miRNA in GBM-EVs, as found for a number of other cell types(Guduric-Fuchs et al., 2012; Li et al., 2013a). Different functions have been attributed to miR-451 including acting as a tumor suppressor(Nan et al., 2010) and deregulating oncogenic pathways (Nan et al., 2010; Tian et al., 2012; Zhang et al., 2012). Thus, this miRNA may be selectively exported to enhance tumor cell growth(Palma et al., 2012). The next most abundant miRNA in GBM-EVs was miR-21, with known oncogenic properties(Krichevsky and Gabriely, 2009). The combined increase in miR-451 and miR-21 in microglia exposed to GBM-EVs in culture presumably contributes to the decrease in their shared target *c-Myc* mRNA, while *in vivo* the decrease in *c-Myc* mRNA in microglia and monocytes/macrophages in the glioma-bearing brain seems to be due primarily to elevation of miR-21. We were unable to detect increased levels of miR-15b, miR-146a and miR-223 in recipient microglia, although these were also high in GBM-EVs (data not shown). The functional activity of specific miRNAs transferred into recipient cells by EVs may depend on the type of particles/vesicles within the EV fraction with which they are associated, the mechanism of uptake of these particles/vesicles by recipient cells, levels of miRNA transferred into the cytoplasm, and levels of the endogenous target mRNAs.

In this study down-regulation of the miR-21 and miR-451 target *c-Myc* mRNA in microglia exposed to GBM-EVs in culture and in microglia/macrophages in glioma-bearing brains supports the functional activity of EV transferred miRNAs, although given other factors transferred by EVs the effect could be indirect. c-MYC is a transcription factor regulating expression of many genes and has been implicated in many biological processes, including growth, energy metabolism, proliferation, differentiation and apoptosis(Conacci-Sorrell et al., 2014). c-MYC does not act as an on-off switch in gene activation, but rather amplifies expression of many genes(Nie et al., 2012). We hypothesize that down-regulation c-MYC expression in microglia and monocytes/macrophages might facilitate shifts in

gene expression patterns that accompany the activation of these cells towards a tumor supportive phenotype(Li and Graeber, 2012; Wei et al., 2013).
By monitoring the levels of specific miRNAs which are inherently the highest in GBM-EVs and their effects on target mRNAs following EV uptake, we have elucidated one of the mechanisms by which GBM cells can influence their microenvironment. Our results confirm that EVs released by glioma cells are taken up by microglia and monocytes/macrophages in culture and within the brain environment *in vivo*. miRNAs which are high in the GBM-EV fraction appear to be transferred intact into recipient microglia and monocytes/macrophages resulting in elevated levels of these miRNAs and down-regulation of a target mRNA. This supports a means of intercellular communication via exRNA in which tumor cells can manipulate the transcriptome of normal cells, as has been described for other miRNAs and non-coding RNAs in glioma and other cancer models(Bronisz et al., 2014; Li et al., 2013a; Zhou et al., 2014).

Materials and Methods

Cell culture

Primary human GBM cells from two patients, 11/5 (GBM1) and 20/3 (GBM2)(Skog et al., 2008), mouse glioma line GL261(Ausman et al., 1970), mouse microglial line KW3 (JEK), primary neonatal mouse microglia and adult human microglia were cultured under standard conditions.
For stimulation experiments, EVs were isolated from 2, 150 mm plates of GBM1 or GBM2 cells (1-2 x 10^{11} EVs) and added to cultures of 0.5 x 10^{5} microglia cells.
GBM2 cells were stably transduced using a CSCW2 lentivector (from Dr. Sena-Esteves) encoding palmitoylated GFP (palmGFP)(Lai et al., 2015). GL261 cells were stably transduced with lentivectors encoding firefly luciferase (Fluc), mCherry (mC) and palmtdTomato (palmdT)(Lai et al., 2015).
Primary mouse microglia were isolated by removal of the brain cortex and dissociating cells by using a 100 μm cell strainer followed by a 40 μm cell strainer. Cells were cultured in DMEM with 10% FBS, 1% P/S and 20 ng/ml M-CSF (Gibco). Primary microglia were harvested from confluent monolayers by shaking off overnight (O/N) and culturing in the same medium.
Primary human microglia were cultured from an autopsy case of a 75-year-old male with de-identified brain tissue collected ~8 h after death due to intraparenchymal brain hemorrhage under an IRB approved protocol. Microglia were isolated from 25 grams of autopsy-derived human cortex using an adaptation of our published mouse protocol(Hickman et al., 2008). Meninges were removed, and tissue was

minced with a sterile razor blade and transferred to a flask containing digestion reagent (RPMI without dye, 20 U/ml collagenase type 3 and 2 U/ml Dispase; Worthington Biochemical Corp). The tissue was incubated for 30 min at 37°C followed by trituration with a 25 ml pipette in which the tip had been broken off leaving a wide bore shaft. DNase I (Roche) was added to a concentration of 40 U/ml and incubated for 20 min. The digested tissue was triturated sequentially with a 25 ml, 10 ml and 5.0 ml pipette and suspension was passed over 100 μm filters. Cells were centrifuged at 300xg for 10 min and the pellet was resuspended in 40 ml PBS/ 5 mM EDTA/10% bovine serum to block enzyme action. Cells were filtered over 70 μm filters, centrifuged 300xg for 10 min, then resuspended in 235 ml 28% Percoll in PBS (Sigma Aldrich). This suspension was centrifuged at 850 x g in a swinging bucket rotor for 40 min with brake set on the lowest setting. Supernatants were removed from all tubes and pellets rinsed twice in cold PBS and pooled. The final pellet was resuspended in MACS buffer (PBS, 0.5% BSA, and 2 mM EDTA) for selection of CD11b+ cells.

CD11b-bearing cells were purified using magnetic bead/column separation (Miltenyi Biotech), according to manufacturer's instructions. Briefly, the cell pellet was resuspended in MACS Buffer, followed by addition of CD11b-Magnetic beads (Miltenyi Biotech) and incubation in the refrigerator for 20 min. Cells were then centrifuged 300 x g for 5 min and the pellet resuspended in 3 ml MACS buffer and passed over an LS column (Miltenyi Biotech) which retained the CD11b bead-bound cells, and eluted with 3 ml MACS buffer. To determine purity of microglia, an aliquot was removed and stained with Alexa-647 labeled rat antiCD11b (Clone M1/70) and Alexa-488 labelled anti-human CD45 (clone H130, both antibodies used at 2 μg/ml, Biolegend). Flow cytometry showed purity of $CD11b^{Hl}$ / $CD45^{mid/Low}$ cells (characteristics of microglia) to be 95%. The purified cells were plated on five T75 flasks in Microglia Medium (ScienCell) containing, penicillin, streptomycin and fungizone (100 IU/ml, 100 μg/ml and 25 μg/ml, respectively; Life Technologies), 5% FBS and 10 ng/ml human Macrophage colony stimulating factor (R&D Systems) and grown for 7 days prior to use.

Isolation of EVs

GBM/glioma cells are cultured in EV-depleted FBS. After 48h, conditioned media was collected and centrifuged for 10 min at 300 xg, 10 min at 2000 xg and the supernatant filtered through 0.8 μm filter (Millipore). EVs were pelleted by centrifugation at 100,000 xg for 80 min in a type 70 Ti rotor (Beckman Coulter). Fractionation of EV pellets was achieved by sucrose density gradient centrifugation.

Visualization of EV uptake in culture and *in vivo*

Primary mouse and human microglia were plated on coverslips coated with poly-L-lysine and incubated with GBM2 palmGFP-EVs or GL261 palmGFP-EVs for 24h. Cells were fixed with 4% paraformaldehyde for 10 min at RT. Coverslips were mounted on slides using prolong Gold antifade reagent with DAPI (Molecular Probes). Vesicle uptake into cells was analyzed by fluorescent microscopy using a Carl Zeiss LSM 5 Pascal laser-scanning confocal microscope. Multiphoton intravital microscopy and immunohistochemistry were used for the direct visualization of EV uptake into cells *in vivo.*

Mouse cytokine array and TGF-β quantification

Primary microglia were cultured with GBM-EVs for 48h, with Brefeldin A (Sigma-Aldrich, 1 µg/ml) added during the last 8h. Cells were lysed and cytokine expression was determined using a Mouse Cytokine Array (R&D Systems). Membranes were scanned and analyzed for pixel intensity using ImageJ. TGF-β in GBM-EVs and microglia was measured by ELISA Human/Mouse TGF-β ELISA Ready-Set-Go kit (eBioscience).

Quantitative Real-Time PCR

Total cellular and EV RNA was isolated with miRNeasy Mini Kit (Qiagen). RNA was concentrated by ethanol precipitation. RNA yields were determined with Nanodrop (Thermo Fisher Scientific); size and quality with 2100 Bioanalyzer (Agilent).

For miRNA analysis of GBM cells and EVs a miRNA expression-profiling panel (1146 miRNAs; Illumina) was used. Individual miRNA expression was analyzed using TaqMan® MicroRNA Assays (Life Technologies) and normalized to U6 RNA.

For quantitative real-time PCR (qRT-PCR) of mRNAs, 50 ng RNA was reverse transcribed using Sensiscript (Qiagen) with Oligo-dT (Roche) and random nanomers (Sigma-Aldrich). qRT-PCR was performed using Power SYBR® Green PCR Master Mix (Invitrogen) (primer sequences in **Supplementary Table 1**). Relative levels of RNA were determined using the comparative ΔCt method. All Ct values were normalized to GAPDH mRNA.

Syngeneic glioma mouse model

Animal experimentation was conducted under the oversight of the Massachusetts

General Hospital Institution Animal Care and Use Committee. *CX3CR1*$^{-GFP/GFP}$ knock-in mice (JEK)(Jung et al., 2000) were bred with *C57BL/6* mice (Charles River Laboratories) and the resulting heterozygous *CX3CR1*$^{GFP/+}$ offspring were used for the intracranial injections of GL261 glioma cells. Brain tumors were generated by intracranial injection of GL261-Fluc-mC-palmtdT cells glioma cells using a stereotactic frame (Harvard Biosciences) into 8-10-week-old heterozygous *CX3CR1*$^{GFP/+}$ mice anaesthetized by subcutaneous injection with ketamine/xylazine. One $\times$ 10^5 tumor cells were injected into the left striatum using the following coordinates: X (lateral) = 0.5 mm, Y (caudal) = 2 mm, Z = 2 mm (deep) from the bregma. Tumor size was monitored by bioluminescence, as previously described.

FACS/RNA analysis

Eighteen days post-tumor injections, the mice were anesthetized and sacrificed by transcardiac perfusion with PBS. Brains were removed and cells processed for FACS using a microglia isolation protocol(Hickman et al., 2008). RNA was isolated from sorted cell fractions for analysis.

Immunoblot

Samples were lysed in RIPA buffer supplemented with a protease inhibitor cocktail (Roche). Total protein concentration was measured using the Biorad protein assay and 20 µg protein was loaded onto pre-cast 4-12% or 10% Bis-Tris Polyacrylamide gel (Invitrogen). Proteins were transferred onto polyvinylidene fluoride membranes (EMD Millipore). Membranes were blocked in 5% non-fat dry milk in TBS-Tween and incubated with antibodies against ALIX (Santa Cruz: sc-53538, 1:500), PTEN (Santa Cruz: sc-6818, 1:200), MIF (Santa Cruz: sc-20121, 1:100), c-MYC (Santa Cruz: sc19, 1:100), GAPDH (Millipore, 1:2000), TGF-β (Cell Signaling, 1:500) and CAB39 (Cell signal, 1:500). Membranes were incubated with their relative horseradish peroxidase - conjugated antibody (1:5000) and imaged using a chemiluminescence detection kit (Thermo Fisher Scientific).

Viability assay

Cell viability was determined using CellTiter-Glo® Luminescent Assay (Promega). Luminescence was measured on a Microtiter Luminometer (Dynex Technologies).

Acetylcholinesterase assay

Isolated EVs were resuspended in PBS, absorbance was measured to establish

a baseline. Acetylthiocholine was added to 1.25 mM in combination with 5,5'-dithiobis(2-nitrobenzoic acid) to 0.1 mM. Change in absorbance was measured at 450 nm every 5 min over 30 min using a MLX microtiter luminometer (Dynex Technologies).

Nanoparticle Tracking Analysis

Number of EVs in PBS was assayed using Nanoparticle Tracking Analysis (NTA) Version 2.2 Build 0375 instrument (NanoSight). Particles were measured for 60 s and number of particles (30 - 800 nm) was determined using NTA Software 2.2.

Isolation of EVs by differential ultracentrifugation

To isolate the EV fraction released by tumor cells, they were cultured in 150 mm culture dishes (BD Falcon). At 50% confluency, cells were washed with PBS and media was replaced by DMEM containing 1% P/S and 5% EV-depleted FBS. After 48h, the conditioned media was collected and the EV fraction was collected by differential centrifugation. The pelleted "EV fraction" (EVs) was resuspended in PBS or DMEM, quantified by Nanosight, analyzed by sucrose density gradient centrifugation, and lysed for RNA and protein determinations. One mg EV protein corresponds to about 10^{11} EV particles.

Isolation of EVs by sucrose gradient-ultracentrifugation

EVs isolated by differential ultracentrifugation were resuspended in PBS and layered on top of a discontinuous sucrose gradient (5%, 10%, 15%, 20%, 25%, 30%, 35%, 40% in PBS), as previously described.[21] Pelleted EVs from different fractions were lysed in Qiazol and both total RNA and protein were isolated. From the aqueous phase RNA was isolated using the miRNeasy Kit, according to manufacturer's protocol. To isolate the protein fraction, 100% EtOH was added to the remaining 0.3 ml Qiazol-chloroform mixture to precipitate the DNA. Next, 1.5 ml isopropanol was added to the supernatant to precipitate proteins and pelleted at 12,000 x g. Pellets were washed thrice with 0.3 M guanidine-hydrochloride in 95% ethanol. Pellets were air-dried and resuspended in 50 µl 1X sample buffer (250 mM TrisHCl pH 6.8, 10% SDS, 30% glycerol, 5% β-mercaptoethanol, 0.02% bromophenol blue) and boiled at 95°C for 5 min.

Multiphoton intravital microscopy of intracranial glioma

Briefly, mice were anesthetized by intraperitoneal injection of ketamine/xylazine, immobilized on a custom-built stereotactic frame and the scalp was incised above

the sagittal suture. The periosteum was removed, and a craniotomy of 4 mm diameter was drilled in one parietal bone. 1 x 10^5 GL261-Fluc-mC-palmtdT were slowly injected intracranially in a 1 µl volume and the craniotomy was closed using a 5 mm coverslip. Mice were allowed to recover for one week before the initiation of imaging. Datasets were collected from 2 weeks after tumor implantation on an Ultima IV multiphoton microscope (Bruker Corporation/Prairie Technologies) using a 20 x 0.95 NA objective lens (Olympus) at 2x-4x optical zoom. Multiphoton excitation of GFP and tdTomato was obtained through a MaiTai DeepSee Ti:Sapphire laser (Newport/Spectra Physics) tuned to 920 nm and a MaiTai Ti:Sapphire laser tuned to 1000 nm. Emitted fluorescence was collected every 15 s through 460/50, 525/50, 595/50, and 660/40 bandpass filters and non-descanned PMTs to create 4-color images. Images were processed into time-lapse movies using Imaris software (Bitplane). To label the blood vasculature, 150 kDa FITC-Dextran (Sigma-Aldrich) was injected intravenously up to 2h prior to imaging.

Visualization of EV uptake *in vivo* using immunohistochemistry

Brains were removed from mice bearing GL261-Fluc-mC-palmtdT tumors and snap frozen in liquid nitrogen with optimal cutting temperature compound (OCT, Thermo Scientific). Embedded brains were cryosectioned (12 microns) and immunostained with rabbit anti-RFP (Cat # ab62341, Abcam) and Alexa Fluor 647 goat anti-rabbit (Life Technologies) antibodies. Samples were imaged using an LSM 710 confocal microscope with a 63x Zeiss Plan-Apochromat SF25, NA1.4 objective (Zeiss).

Buffer compositions

RIPA buffer (20 mM Tris, pH 7.4, 150 mM NaCl, 1% NP-40, 0.1% SDS 0.5% sodium deoxycholine, 5 mM EDTA). EV depleted FBS, serum was ultracentrifuged at 100,000 x g for 16h, and the supernatant sterilized by filtration through 0.2 µm filters.

Statistical analysis

The unpaired 2-sample t test was used to compare between 2 groups. One-way ANOVA, followed by Bonferroni's test, was conducted to test for significance among multiple groups, comparing all pairs of columns.

References

Arroyo, J.D., Chevillet, J.R., Kroh, E.M., Ruf, I.K., Pritchard, C.C., Gibson, D.F., Mitchell, P.S., Bennett, C.F.,

Pogosova-Agadjanyan, E.L., Stirewalt, D.L.*, et al.* (2011). Argonaute2 complexes carry a population of circulating microRNAs independent of vesicles in human plasma. Proc Natl Acad Sci U S A *108*, 5003-5008.

Atai, N.A., Balaj, L., van Veen, H., Breakefield, X.O., Jarzyna, P.A., Van Noorden, C.J., Skog, J., and Maguire, C.A. (2013). Heparin blocks transfer of extracellular vesicles between donor and recipient cells. J Neurooncol *115*, 343-351.

Ausman, J.I., Shapiro, W.R., and Rall, D.P. (1970). Studies on the chemotherapy of experimental brain tumors: development of an experimental model. Cancer Res *30*, 2394-2400.

Balaj, L., Lessard, R., Dai, L., Cho, Y.-J., Pomeroy, S.L., Breakefield, X.O., and Skog, J. (2011). Tumour microvesicles contain retrotransposon elements and amplified oncogene sequences. Nature Communications *2*, 180.

Betel, D., Koppal, A., Agius, P., Sander, C., and Leslie, C. (2010). Comprehensive modeling of microRNA targets predicts functional non-conserved and non-canonical sites. Genome Biol *11*, R90.

Bobrie, A., Krumeich, S., Reyal, F., Recchi, C., Moita, L.F., Seabra, M.C., Ostrowski, M., and Thery, C. (2012). Rab27a supports exosome-dependent and -independent mechanisms that modify the tumor microenvironment and can promote tumor progression. Cancer Res *72*, 4920-4930.

Bronisz, A., Wang, Y., Nowicki, M.O., Peruzzi, P., Ansari, K., Ogawa, D., Balaj, L., De Rienzo, G., Mineo, M., Nakano, I.*, et al.* (2014). Extracellular vesicles modulate the glioblastoma microenvironment via a tumor suppression signaling network directed by miR-1. Cancer Res *74*, 738-750.

Cocco, C., Pistoia, V., and Airoldi, I. (2012). Anti-leukemic properties of IL-12, IL-23 and IL-27: differences and similarities in the control of pediatric B acute lymphoblastic leukemia. Crit Rev Oncol Hematol *83*, 310-318.

Conacci-Sorrell, M., McFerrin, L., and Eisenman, R.N. (2014). An overview of MYC and its interactome. Cold Spring Harb Perspect Med *4*, a014357.

Coniglio, S.J., and Segall, J.E. (2013). Review: molecular mechanism of microglia stimulated glioblastoma invasion. Matrix Biol *32*, 372-380.

D'Asti, E., Garnier, D., Lee, T.H., Montermini, L., Meehan, B., and Rak, J. (2012). Oncogenic extracellular vesicles in brain tumor progression. Front Physiol *3*, 294.

de Vrij, J., Maas, S.L., Kwappenberg, K.M., Schnoor, R., Kleijn, A., Dekker, L., Luider, T.M., de Witte, L.D., Litjens, M., van Strien, M.E.*, et al.* (2015). Glioblastoma-derived extracellular vesicles modify the phenotype of monocytic cells. Int J Cancer *137*, 1630-1642.

Ellert-Miklaszewska, A., Dabrowski, M., Lipko, M., Sliwa, M., Maleszewska, M., and Kaminska, B. (2013). Molecular definition of the pro-tumorigenic phenotype of glioma-activated microglia. Glia *61*, 1178-1190.

Gabrusiewicz, K., Ellert-Miklaszewska, A., Lipko, M., Sielska, M., Frankowska, M., and Kaminska, B. (2011). Characteristics of the alternative phenotype of microglia/macrophages and its modulation in experimental gliomas. PloS one *6*, e23902.

Guduric-Fuchs, J., O'Connor, A., Camp, B., O'Neill, C.L., Medina, R.J., and Simpson, D.A. (2012). Selective extracellular vesicle-mediated export of an overlapping set of microRNAs from multiple cell types. BMC Genomics *13*, 357.

Hickman, S.E., Allison, E.K., and El Khoury, J. (2008). Microglial dysfunction and defective beta-amyloid clearance pathways in aging Alzheimer's disease mice. The Journal of neuroscience : the official journal of the Society for Neuroscience *28*, 8354-8360.

Hickman, S.E., Kingery, N.D., Ohsumi, T.K., Borowsky, M.L., Wang, L.-c., Means, T.K., and El Khoury, J. (2013). The microglial sensome revealed by direct RNA sequencing. Nature Neuroscience *16*, 1896-1905.

Johnson, D.R., and O'Neill, B.P. (2012). Glioblastoma survival in the United States before and during the temozolomide era. J Neurooncol *107*, 359-364.

Jung, S., Aliberti, J., Graemmel, P., Sunshine, M.J., Kreutzberg, G.W., Sher, A., and Littman, D.R. (2000). Analysis of fractalkine receptor CX(3)CR1 function by targeted deletion and green fluorescent protein reporter gene insertion. Mol Cell Biol *20*, 4106-4114.

Krichevsky, A.M., and Gabriely, G. (2009). miR-21: a small multi-faceted RNA. J Cell Mol Med *13*, 39-53.

Kushchayev, S.V., Kushchayeva, Y.S., Wiener, P.C., Scheck, A.C., Badie, B., and Preul, M.C. (2014). Monocyte-derived cells of the brain and malignant gliomas: the double face of Janus. World Neurosurg *82*, 1171-1186.

Lai, C.P., Kim, E.Y., Badr, C.E., Weissleder, R., Mempel, T.R., Tannous, B.A., and Breakefield, X.O. (2015). Visualization and tracking of tumour extracellular vesicle delivery and RNA translation using multiplexed reporters. Nature Communications *6*, 7029.

Li, C.C., Eaton, S.A., Young, P.E., Lee, M., Shuttleworth, R., Humphreys, D.T., Grau, G.E., Combes, V., Bebawy, M., Gong, J.*, et al.* (2013a). Glioma microvesicles carry selectively packaged coding and non-coding RNAs which alter gene expression in recipient cells. RNA Biol *10*, 1333-1344.

Li, H.P., Zeng, X.C., Zhang, B., Long, J.T., Zhou, B., Tan, G.S., Zeng, W.X., Chen, W., and Yang, J.Y. (2013b). miR-451 inhibits cell proliferation in human hepatocellular carcinoma through direct suppression of IKK-beta. Carcinogenesis *34*, 2443-2451.

Li, W., and Graeber, M.B. (2012). The molecular profile of microglia under the influence of glioma. Neuro-oncology *14*, 958-978.

Li, X., Sanda, T., Look, A.T., Novina, C.D., and von Boehmer, H. (2011). Repression of tumor suppressor miR-451 is essential for NOTCH1-induced oncogenesis in T-ALL. J Exp Med *208*, 663-675.

Manterola, L., Guruceaga, E., Gallego Perez-Larraya, J., Gonzalez-Huarriz, M., Jauregui, P., Tejada, S., Diez-Valle, R., Segura, V., Sampron, N., Barrena, C.*, et al.* (2014). A small noncoding RNA signature found in exosomes of GBM patient serum as a diagnostic tool. Neuro Oncol *16*, 520-527.

Meng, F., Henson, R., Wehbe-Janek, H., Ghoshal, K., Jacob, S.T., and Patel, T. (2007). MicroRNA-21 regulates expression of the PTEN tumor suppressor gene in human hepatocellular cancer. Gastroenterology *133*, 647-658.

Nan, Y., Han, L., Zhang, A., Wang, G., Jia, Z., Yang, Y., Yue, X., Pu, P., Zhong, Y., and Kang, C. (2010). MiRNA-451 plays a role as tumor suppressor in human glioma cells. Brain Res *1359*, 14-21.

Nie, Z., Hu, G., Wei, G., Cui, K., Yamane, A., Resch, W., Wang, R., Green, D.R., Tessarollo, L., Casellas, R.*, et al.* (2012). c-Myc is a universal amplifier of expressed genes in lymphocytes and embryonic stem cells. Cell *151*, 68-79.

Palma, J., Yaddanapudi, S.C., Pigati, L., Havens, M.A., Jeong, S., Weiner, G.A., Weimer, K.M., Stern, B., Hastings, M.L., and Duelli, D.M. (2012). MicroRNAs are exported from malignant cells in customized particles. Nucleic Acids Res *40*, 9125-9138.

Pan, X., Wang, R., and Wang, Z.X. (2013). The potential role of miR-451 in cancer diagnosis, prognosis, and therapy. Mol Cancer Ther *12*, 1153-1162.

Peinado, H., Aleckovic, M., Lavotshkin, S., Matei, I., Costa-Silva, B., Moreno-Bueno, G., Hergueta-Redondo, M., Williams, C., Garcia-Santos, G., Ghajar, C.*, et al.* (2012). Melanoma exosomes educate bone marrow progenitor cells toward a pro-metastatic phenotype through MET. Nat Med *18*, 883-891.

Richmond, J., Tuzova, M., Cruikshank, W., and Center, D. (2014). Regulation of cellular processes by interleukin-16 in homeostasis and cancer. J Cell Physiol *229*, 139-147.

Ries, C. (2014). Cytokine functions of TIMP-1. Cell Mol Life Sci *71*, 659-672.

Skog, J., Würdinger, T., van Rijn, S., Meijer, D.H., Gainche, L., Sena-Esteves, M., Curry, W.T., Carter, B.S., Krichevsky, A.M., and Breakefield, X.O. (2008). Glioblastoma microvesicles transport RNA and proteins that promote tumour growth and provide diagnostic biomarkers. Nat Cell Biol *10*, 1470-1476.

Tian, Y., Nan, Y., Han, L., Zhang, A., Wang, G., Jia, Z., Hao, J., Pu, P., Zhong, Y., and Kang, C. (2012). MicroRNA miR-451 downregulates the PI3K/AKT pathway through CAB39 in human glioma. Int J Oncol *40*, 1105-1112.

Verhaak, R.G., Hoadley, K.A., Purdom, E., Wang, V., Qi, Y., Wilkerson, M.D., Miller, C.R., Ding, L., Golub, T., Mesirov, J.P.*, et al.* (2010). Integrated genomic analysis identifies clinically relevant subtypes of glioblastoma characterized by abnormalities in PDGFRA, IDH1, EGFR, and NF1. Cancer Cell *17*, 98-110.

Vickers, K.C., Palmisano, B.T., Shoucri, B.M., Shamburek, R.D., and Remaley, A.T. (2011). MicroRNAs are transported in plasma and delivered to recipient cells by high-density lipoproteins. Nat Cell Biol *13*, 423-433.

Wei, J., Gabrusiewicz, K., and Heimberger, A. (2013). The controversial role of microglia in malignant gliomas. Clin Dev Immunol *2013*, 285246.

Weinstein, J.N., Myers, T.G., O'Connor, P.M., Friend, S.H., Fornace, A.J., Jr., Kohn, K.W., Fojo, T., Bates, S.E., Rubinstein, L.V., Anderson, N.L*., et al.* (1997). An information-intensive approach to the molecular pharmacology of cancer. Science *275*, 343-349.

Wurdinger, T., Deumelandt, K., van der Vliet, H.J., Wesseling, P., and de Gruijl, T.D. (2014). Mechanisms of intimate and long-distance cross-talk between glioma and myeloid cells: how to break a vicious cycle. Biochim Biophys Acta *1846*, 560-575.

Zhang, Z., Luo, X., Ding, S., Chen, J., Chen, T., Chen, X., Zha, H., Yao, L., He, X., and Peng, H. (2012). MicroRNA-451 regulates p38 MAPK signaling by targeting of Ywhaz and suppresses the mesangial hypertrophy in early diabetic nephropathy. FEBS Lett *586*, 20-26.

Zhou, W., Fong, M.Y., Min, Y., Somlo, G., Liu, L., Palomares, M.R., Yu, Y., Chow, A., O'Connor, S.T., Chin, A.R*., et al.* (2014). Cancer-secreted miR-105 destroys vascular endothelial barriers to promote metastasis. Cancer Cell *25*, 501-515.

Supplementary information

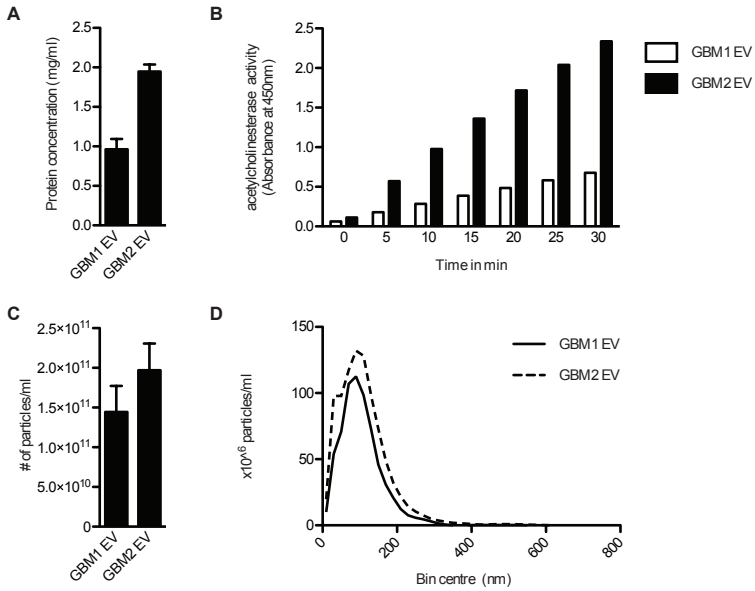

Supplementary Figure S1. GBM cells secrete large quantities of EVs. (A, B, C, D) EVs were isolated from 2 primary human GBM cell lines, GBM1 and GBM2 by differential ultracentrifugation and resuspended in PBS. **(A)** The protein concentration (mg/ml) was measured by Bradford assay. Data presented of 2 independent samples with technical quadruples. **(B)** Number of EVs released over time was measured using an acetylcholinesterase assay by absorbance at 450 nm. **(C)** The number of EVs released by the different cells was measured by nanotracking the particles with Nanosight as the average number of particles in 2 independent samples isolated from the two cell lines. **(D)** The size distribution of particles was measured by Nanosight particle tracking.

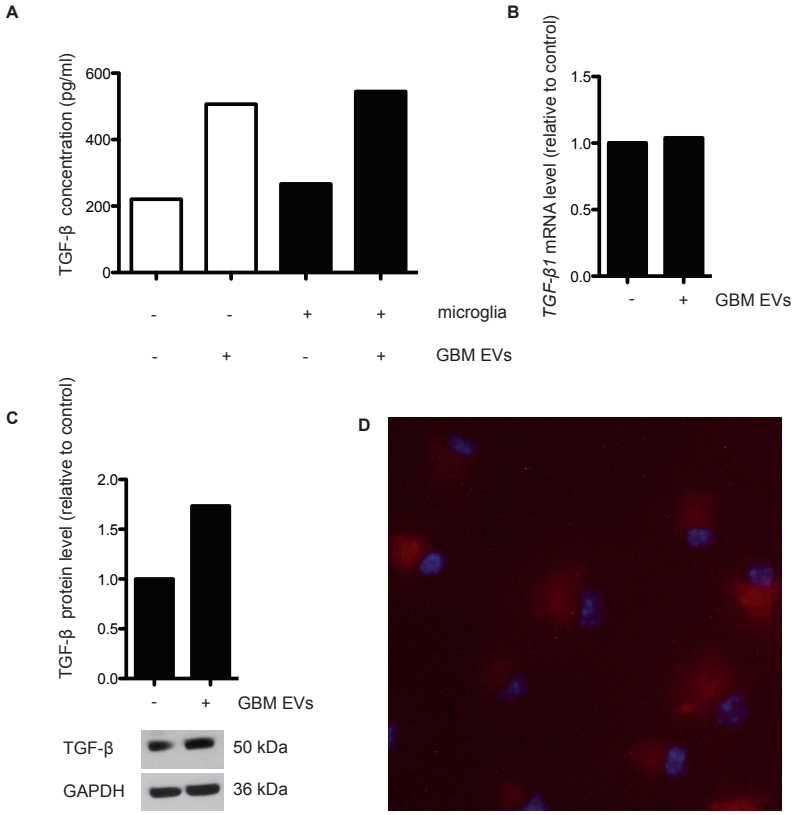

Supplementary Figure S2. **TGF-β is present in vesicles and is transferred to primary mouse microglia.** (**A**) GBM-EVs were added to wells containing no cells or wells containing primary mouse microglial cells. After 48h TGF-βlevels were quantified using an ELISA assay. TGF-β levels in culture media without primary mouse microglial cells, without or with the addition of GBM-EVs for 48h, was determined with an ELISA assay. Protein concentration of TGF-β are presented in pg/ml. (**B**) Relative mRNA levels of *Tgf-β* were analyzed using quantitative RT-PCR and primers specific to the mouse message. Levels were normalized to *Gapdh* mRNA, and fold expression presented where 1.0-fold corresponds to 22.3 Ct. (**C**) Western blot analysis of TGF-β levels in primary mouse microglial cells after 48h with and without GBM-EVs. (**D**) EVs were isolated from GL261 cells expressing Fluc-mC-palmtdT by differential ultracentrifugation and incubated with primary human microglia. After 24h cells were fixed, stained with DAPI and analyzed by confocal fluorescent microscopy using a 20X objective.

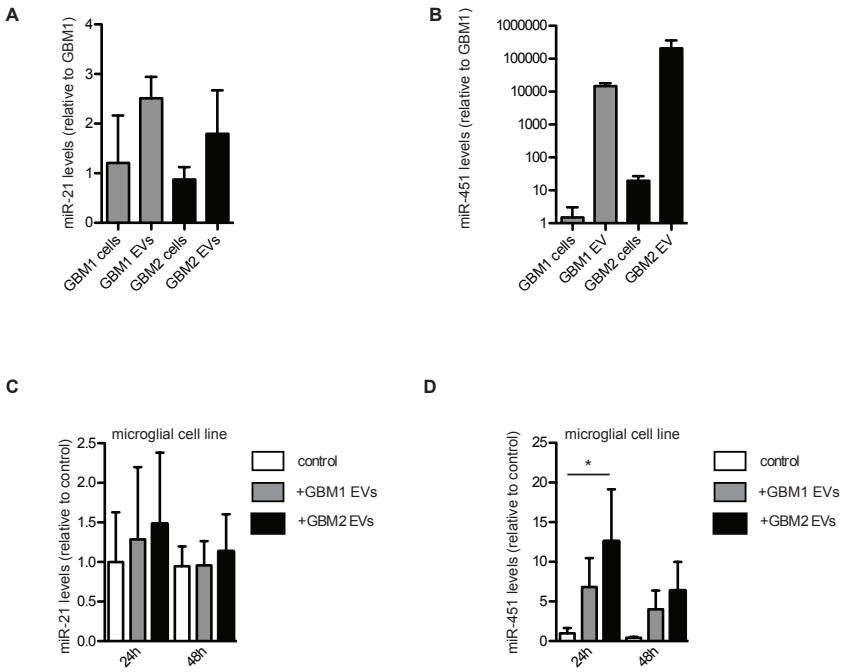

Supplementary Figure S3. GBM-derived EVs increase miR-21 and miR-451 levels in a mouse microglia cell line. (A, B): EVs released by primary human GBM cell lines were isolated by differential centrifugation, and total RNA was isolated from EVs as well from the donor cells. Relative levels of miR-21 **(A)** and miR-451 **(B)** were analyzed using TaqMan® assays. Data are represented as mean ± SEM normalized for U6 (n=2). Fold expression is presented where 1.0-fold corresponds to 18 Ct for miR-21 and 36 Ct for miR-451. **(C, D)**: **A** microglia cell line was exposed to EVs isolated from two primary GBM cell lines. Relative levels of miR-21 **(C)** and miR-451 **(D)** were analyzed using TaqMan® assays. Data are represented as mean ± SEM normalized to U6 (n=5). * $p < 0.05$. Fold expression is presented where 1.0-fold corresponds to a normalized Ct value 19.8 for miR-21 and 35.5 for miR-451.

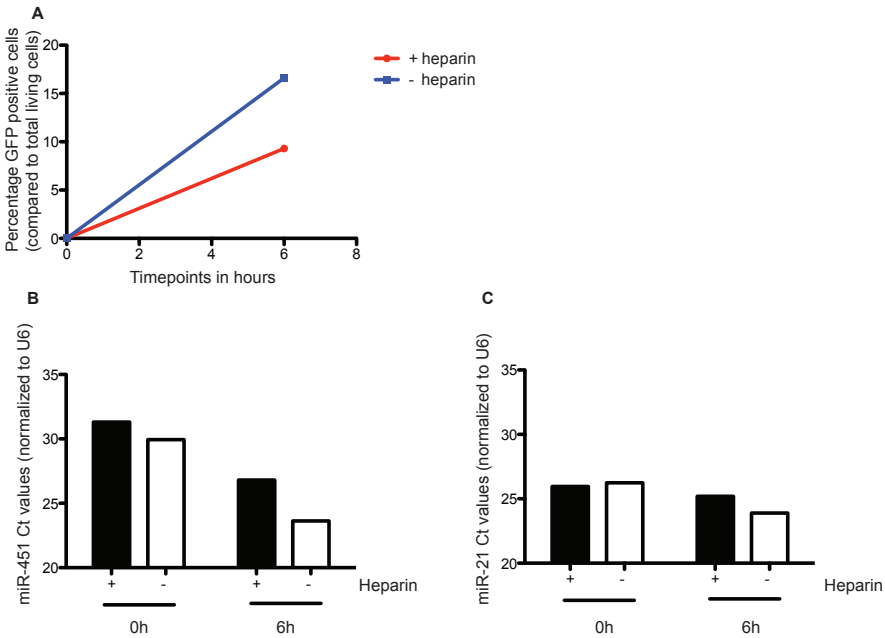

Supplementary Figure S4. **Heparin interferes with the uptake of GBM-EVs and reduces the transfer of miRNA.** Based on published studies demonstrating that heparin can block uptake of EVs(Atai et al., 2013): (**A**) primary mouse microglial cells were exposed to EVs isolated from palmGFP-GBM2 cells with or without the addition of heparin (final concentration 200 µg/ml). Cells are collected 0 and 6 h after exposure to vesicles. Percentage of cells made GFP+ through uptake of vesicles compared to the total living cells per condition (with or without heparin) was analyzed by FACS. (**B, C**): Total RNA was isolated and miRNA expression was determined with Taqman qPCR. Relative levels of miR-451 (**B**) and miR-21 (**C**) in GFP^+ cells were analyzed using TaqMan® assays and the data normalized to U6.

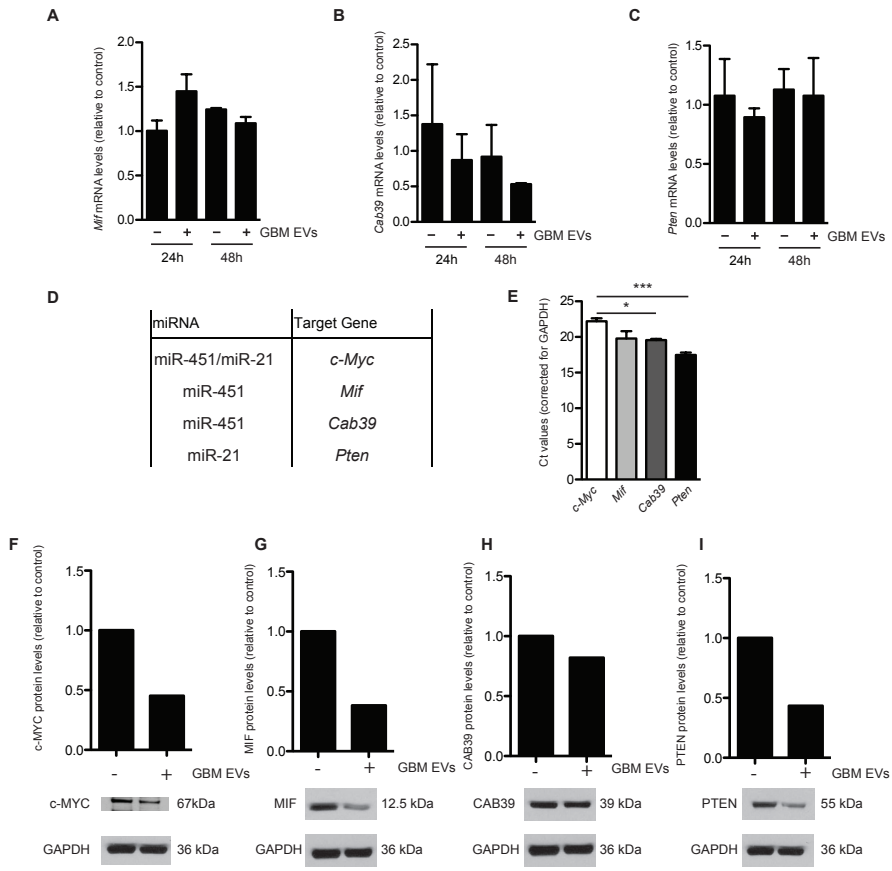

Supplementary Figure S5. GBM-derived EVs do not affect mRNA levels of *Cab39, Mif* and *Pten.* (A-C): Primary mouse microglia were exposed to GBM2 EVs. Relative mRNA levels of *Cab39* **(A)**, *Mif* **(B)**, and *Pten* **(C)** were analyzed using quantitative RT-PCR. Data are represented as mean ± SEM normalized to *Gapdh* mRNA (n=3). **(D)** Table shows the validated targets of mi-R451 and/or miR-21, as described in the literature(Li et al., 2013b; Li et al., 2011). **(E).** Depicted are the Ct values for *c-Myc, Cab39*, *Mif* and *Pten* calculated in the mouse microglia (levels determined after 24h in culture without exposure to GBM vesicles). Data are represented as mean ± SEM normalized for *Gapdh* mRNA (n=2). * $p < 0.05$, *** $p < 0.001$. (**F, G, H, I**) Primary mouse microglia were exposed to GBM-EVs. After 48h cells were lysed and relative protein levels of c-Myc (**F**), Pten (**F**), Mif (**G**) and Cab39 (**H**) were analyzed using western blotting. The expression levels were quantified by densitometric analysis using ImageJ. Data are normalized to Gapdh.

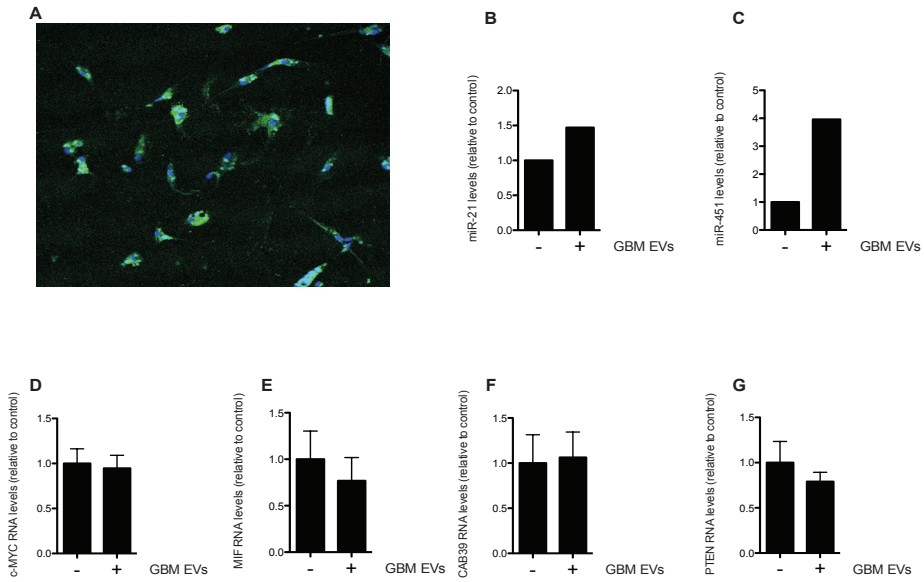

Supplementary Figure S6. Effect of GBM-derived EVs on miR-21 and miR-451 levels and target mRNA levels in primary human microglia. (**A**) EVs were isolated from GBM2 cells expressing palmGFP by differential ultracentrifugation and incubated with primary human microglia at 60% confluence. After 24h cells were fixed, stained with DAPI and analyzed by confocal fluorescent microscopy using a 20X objective. (**B, C**) Primary human microglia were exposed to GBM-EVs for 48h. Relative levels of miR-21 (**B**) and miR-451 (**C**) were analyzed using TaqMan® assays. Fold expression is presented where 1.0-fold corresponds to Ct values of 20.2 for miR-21 and 33.3 for miR-451 normalized to U6 RNA. (**D-G**) Primary human microglia were exposed to GBM-EVs isolated from human palmGFP-GBM2 cells for 48h. Relative mRNA levels of *c-MYC* (**D**), *MIF* (**E**), *CAB39* (**F**) and *PTEN* (**G**) were analyzed using quantitative RT-PCR and normalized to *GAPDH* mRNA. Fold expression is presented where 1.0-fold corresponds to 27 for *c-MYC*, 21.8 for *MIF*, 24 for *CAB39* and 25 for *PTEN* in normalized Ct values.